Arabian Journal of Chemistry (2020) **13**, 5923–5938

King Saud University

Arabian Journal of Chemistry

www.ksu.edu.sa
www.sciencedirect.com

ORIGINAL ARTICLE

Polysaccharide/Fe(III)-porphyrin hybrid film as catalyst for oxidative decolorization of toxic azo dyes: An approach for wastewater treatment

Henrique P. Mota [a], Rafael F.N. Quadrado [a], Thiago A.L. Burgo [b], Bernardo A. Iglesias [c,*], André R. Fajardo [a,*]

[a] *Laboratório de Tecnologia e Desenvolvimento de Compósitos e Materiais Poliméricos (LaCoPol), Universidade Federal de Pelotas (UFPel), Campus Capão do Leão s/n, 96010-900 Pelotas-RS, Brazil*
[b] *Departamento de Física, Universidade Federal de Santa Maria, Av. Roraima 1000, Campus Camobi, 97105-900, Santa Maria RS, Brazil*
[c] *Laboratório de Bioinorgânica e Materiais Porfirínicos, Departamento de Química, Universidade Federal de Santa Maria, Av. Roraima 1000, Campus Camobi, 97105-900 Santa Maria-RS, Brazil*

Received 29 January 2020; accepted 20 April 2020
Available online 28 April 2020

KEYWORDS

Hybrid materials;
Heterogeneous catalysis;
Chitosan;
Metalloporphyrins;
Azo dyes;
Wastewater treatment

Abstract A hybrid film of chitosan/poly(vinyl alcohol)/cationic Fe(III)-porphyrin (Cht/PVA-FeTMPyP) was synthesized to act as a Fenton-like catalyst to decolorize methyl orange and methyl red azo dyes. The Cht/PVA-FeTMPyP film was characterized by different analytical and microscopy techniques, which indicated that the metalloporphyrin affects different properties of the hybrid film. Batch experiments revealed that the hybrid film exhibits enhanced catalytic activity towards dyes decolorization in the presence of H_2O_2 as compared to the "free" FeTMPyP. Fast decolorization rates as high as 90 min were observed for both azo dyes under mild conditions (pH 7 and room temperature), even at low concentrations of the catalyst in H_2O_2. After the decolorization, FTIR analysis showed that simple molecules are released as by-products. Moreover, the hybrid film performed well in cyclic runs without leaching out iron ions or losing its catalytic activity. All these features associated with its ease handling ranks the Cht/PVA-FeTMPyP hybrid film as a promising heterogeneous Fenton-like catalyst for the decomposition of azo dyes in water.
© 2020 Published by Elsevier B.V. on behalf of King Saud University. This is an open access article under the CC BY-NC-ND license (http://creativecommons.org/licenses/by-nc-nd/4.0/).

* Corresponding authors.
E-mail addresses: bernardopgq@gmail.com (B.A. Iglesias), andre.fajardo@pq.cnpq.br (A.R. Fajardo).
Peer review under responsibility of King Saud University.

ELSEVIER Production and hosting by Elsevier

1. Introduction

Synthetic dyes are among the most harmful chemical pollutants present in the water. In fact, due to their extensive use in textile and finishing industries, millions of gallons of these effluents are discharged in the water bodies. Consequently, the presence of these pollutants in water causes several

https://doi.org/10.1016/j.arabjc.2020.04.021
1878-5352 © 2020 Published by Elsevier B.V. on behalf of King Saud University.
This is an open access article under the CC BY-NC-ND license (http://creativecommons.org/licenses/by-nc-nd/4.0/).

environmental damages and various types of risks to human health, either directly or indirectly (Berradi et al., 2019; Holkar, et al., 2016).

Azo dyes, a class of synthetic dyes, have lately attracted much attention from environmental researchers due to their detrimental features and long-lasting persistence in aquatic environments. Also, azo dyes exhibit high light stability and wash fastness, while having resistance to microbial degradation (Chung, 2016). Moreover, chemical composition involving aromatic rings, azoic linkages, and amino groups increase the harmful characteristics of these compounds to nature (Xia et al., 2020). In light of these considerations, azo dyes are not readily removed from wastewater by conventional treatment technologies. Among the methods tested to solve this striking and challenging issue, techniques involving adsorptive processes, decolorization by photocatalysis or oxidative methods and enzymatic decomposition seem to be the most promising approaches (Dong et al., 2015).

Advanced oxidative processes (AOP) using hydrogen peroxide (H_2O_2) in the presence of iron species (Fe(II) or Fe (III)) have been frequently applied to decolorize azo dyes in water (Gao et al., 2020; Zhang and Zhou, 2019). These reactions, known as Fenton or Fenton-like reactions, involve the generation of hydroxyl radicals (•OH) from H_2O_2 mediated by Fe(II)/(III) ions, which oxidize the azo dye molecules (Ali et al., 2013). Currently, the use of Fenton reactions to decolorize azo dyes faces two main challenges to overcome: the reduction of the concentration of iron required to decolorize the dye efficiently a simplified method to recovery the precipitated catalyst from the treated effluent.

Heterogeneous Fenton catalysts seem to be an attractive approach for the above-described limitations. In fact, Fe-containing materials have shown remarkable potential in Fenton reactions since the catalytic activity of the iron ions is maximized while making the recovery from the reaction system feasible (Hassan and Hameed, 2011; Quadrado and Fajardo, 2017). Besides, the entrapment of iron ions on solid supports is a convenient way to avoid the leaching of catalysts, preventing secondary pollution (Huang et al., 2019; Jin et al., 2020).

Within this context, we describe the synthesis of a hybrid film based on a polymer matrix embedded with a pentacationic 5,10,15,20-tetrakis(*N*-methyl-4-pyridyl)porphyrin-Fe(III) tetrachloride (denoted as FeTMPyP) to act as a Fenton-like catalyst for decolorization of azo dyes (Emmert et al., 2008; Parra et al., 2004). Herein, a chitosan and poly(vinyl alcohol) blend was used polymer matrix. Chitosan (Cht), a well-known polysaccharide is widely applied as supporting material due to its chelating nature, and poly(vinyl alcohol) (PVA) has excellent film-forming properties, and both were utilized to synthesize the polymer supporting matrix (Kumar et al., 2019; Souza et al., 2019). Overall, metalloporphyrins have an essential role in a variety of chemical and biochemical processes (da Silva et al., 2014; Tagliatesta et al., 2002). In particular, Fe-porphyrins are famous due to their catalytic activity in oxidative processes, which are employed in organic-synthesis and degradation reactions (Devi and Nithya, 2018; Saltarelli et al., 2019). The use of metalloporphyrins in oxidative processes also have gained spread attention in the past few years due to their advantages, such as: (i) they are stable compounds that can be stabilized on surfaces by electrostatic forces (cationic porphyrins) or by covalent forces; (ii) in the presence of adequate irradiation conditions, they can generate reactive oxygen species with great efficiencies, such as singlet oxygen and/or radical species; (iii) metalloporphyrins incorporated into polymeric materials or solid supports provide more applicability in terms of advanced oxidative processes, making these hybrid materials easy to remove and reuse; and (iv) metalloporphyrins are biomimetic models and can perform oxidation reactions with great ease, mainly porphyrins containing Fe(III) or Mn(III) (like-P450 model) (Rayati and Sheybanifard, 2016; Ucoski et al., 2015; Zucca et al., 2012).

The use of Fe-porphyrins in homogeneous catalysis shows some limitations associated with deactivation, recovery, and reuse issues. Thus, the immobilization of these porphyrins into solid support has been reported as an effective strategy to increase their stability and applicability (Gao et al., 2020). Based on these characteristics, here we show that the Cht/PVA film can act as efficient support to the FeTMPyP, enhancing its catalytic activity in Fenton-like reactions and sufficiently fast in the decolorization of methyl orange (MO) and methyl red (MR) azo dyes. Also, this approach can be a useful strategy to reduce the amount of iron used to catalyze the generation of oxidant species.

2. Materials and methods

2.1. Materials

The materials used in this work are detailed in the Supplementary material.

2.2. Synthesis of the hybrid film

Hybrid films consisting of Cht/PVA embedded with cationic FeTMPyP were prepared by the solvent casting method (de Souza et al., 2017). For this, Cht (600 mg) was solubilized in acetic acid solution (30 mL, 1 v/v-%) at 25 °C for 4 h, while PVA (400 mg) was solubilized in distilled water (20 mL, 80 °C for 6 h). Later, the PVA solution was cooled down to room temperature and added to the Cht solution. The resulting system was blended and homogenized for 30 min. Next, FeTMPyP (1.0 mg) was added to the polymeric solution, and the system was homogenized under magnetic stirring for more 15 min. This mass ratio between the polymers and porphyrin was selected from previous experiments that showed higher FeTMPyP concentrations impairs the film properties. In comparison, lower porphyrin concentrations result in reduced catalytic activity. Next, glutaraldehyde (80 μL), the crosslinker, was added by dropwise to the solution, which was homogenized for 5 min. Then, the filmogenic solution was poured into Petri dishes (round-plate shape 85 × 10 mm) that were left in the oven (40 °C for 24 h) to evaporate the solvent. The resulting film was peeled off the Petri dishes and thoroughly washed with distilled water up to neutral pH. Finally, the film was oven-dried (40 °C for 24 h) and stored in dissector prior use. It is worth to mention that the distilled water used to wash the film was further analyzed by UV–Vis spectroscopy. No absorption band of FeTMPyP was observed (Fig. S1). Therefore, the amount of porphyrin loaded on the film sample was estimated to be 1 mg/g. For comparative purposes, a film sample without FeTMPyP was prepared using a similar protocol. The samples were denoted as Cht/PVA and Cht/PVA-FeTMPyP, respectively.

2.3. Characterization

The characterization techniques and assays can be found in the Supplementary material.

2.4. Decolorization experiments

The decolorization of the two azo dyes (MO and MR) in aqueous medium using the Cht/PVA-FeTMPyP film as the catalyst of a Fenton-like reaction was performed as follows: The catalyst was put in a conical flask (100 mL) filled with 25 mL of MO or MR aqueous solutions. The flasks were placed on an orbital shaker (100 rpm) at 25 °C under ambient light conditions. The reaction was initiated after the addition of H_2O_2, and the decolorization process was monitored using a UV–Visible Perkin Elmer Lambda 24 spectrophotometer (USA). Aliquots of 4 mL were withdrawn from the reaction flasks at desired time intervals and analyzed. The absorbances of MO and MR were measured at wavelengths of 464 nm and 430 nm, respectively. After that, the aliquots were returned to the reaction flasks. Eq. (1) was used to calculate the decolorization ratio of each azo dye:

$$Decolorization\ \ rate = \frac{A_t}{A_o} \quad (1)$$

where A_o is the initial absorbance of each azo dye solution ($t \approx 0$ min) and A_t is the absorbance at $t \neq 0$. All the experiments were performed in triplicates (n = 3). The effects of the initial dye concentration (1–20 ppm), pH (3–7), H_2O_2 concentration (1–20 mmol/L), and catalyst dosage (60–100 mg) on the MO and MR decolorization processes were investigated. For comparative purposes, additional decolorization experiments were performed using the Cht/PVA film and "free" FeTMPyP as catalysts. Briefly, these experiments were performed by using the procedures as described above; however, when "free" FeTMPyP was used (60 μg), it was added to the reaction medium directly. Control experiments were also performed under similar experimental conditions but in the absence of a catalyst.

2.5. Reuse experiments

Consecutive decolorization reactions were performed to investigate the stability and reusability of the Cht/PVA-FeTMPyP film. For this, a unique sample was used in five consecutive decolorization reactions. The experimental conditions of each reaction were set as: catalyst dosage – 60 mg; solution volume – 25 mL; initial dye concentration – 10 ppm; pH – 7; H_2O_2 concentration – 1 mmol/L; room temperature; and reaction time – 90 min. The catalyst was recovered after each reaction, washed in distilled water, and oven-dried (50 °C overnight). Then, it was reused in another reaction run. After each reaction, the decolorization efficiency was computed as described in the previous section.

3. Results and discussion

3.1. Characterization of the hybrid films

The FTIR spectra of Cht, PVA, FeTMPyP, Cht/PVA, and Cht/PVA-FeTMPyP are shown in Fig. 1a. The FeTMPyP spectrum exhibited a broad band centered at 3382 cm^{-1} (ascribed to the absorbed moisture) and its typical bands at 1614 cm^{-1} (C═N stretch from pyridyl rings), 1537 cm^{-1} (C═C stretch vibrations), 1169 cm^{-1} (in-plane N—H bending), 995 cm^{-1} (C-H rocking vibration), and 852 cm^{-1} (out-of-plane C—H bending) (He et al., 2012; Wang et al. 2014a, b). The FTIR spectrum of Cht exhibited a broad band centered at 3440 cm^{-1} (O—H stretching overlapping the N—H stretching) and bands in the range 2970–2830 cm^{-1} (C—H symmetric stretching). Also, bands at 1660 cm^{-1} (C═O stretching of amide I), 1594 cm^{-1} (N-H deformation of amide II), 1425 cm^{-1} (C—N stretching), 1330 cm^{-1} (C—OH stretching) and 1083 cm^{-1} (C—O—C stretching of glycosidic bonds) were observed (de Souza et al., 2017). The PVA spectrum exhibited a broad band centered at 3472 cm^{-1} (O—H stretching); bands in the region 2980–2800 cm^{-1} (C—H stretching of alkyl groups), at 1710 cm^{-1} (C═O stretching of residual acetate groups) and a sharp band at 1095 cm^{-1} (C—O stretching) (de Souza et al., 2017). The FTIR spectrum of the Cht/PVA film exhibited the characteristic bands proceeding from Cht and PVA and some discrepancies as compared to the Cht spectrum due to the chemical cross-linking with glutaraldehyde. The glutaraldehyde is a dialdehyde that reacts with the free amino groups of Cht or with the hydroxyl groups of PVA, forming imine, and acetal bonds (de Souza et al., 2017). As shown in Fig. 1a, the Cht/PVA spectrum has a shoulder-type band at 1642 cm^{-1} associated with the imine bond (C═N stretching) formed between the Cht and glutaraldehyde. Also, the low-intensity band at 1154 cm^{-1} can be assigned to the acetal bond formed between PVA and the glutaraldehyde (Pawar and Yadav, 2014), while the shoulder-type band at 1539 cm^{-1} is attributed to the ethylenic bond of glutaraldehyde (de Souza et al., 2017). Furthermore, the bands associated with the functional groups that participated in this reaction (amino and hydroxyl groups) were shifted to higher wavenumber region (O—H and N—H stretching band to 3447 cm^{-1} and C—N stretching band to 1445 cm^{-1}, respectively). Overall, these findings confirm the crosslinking process.

After the immobilization of the FeTMPyP into the polymeric matrix, some changes in the film spectrum can be noted, as observed in Fig. 1a. The main differences are related to the shifting of the band at 3447 cm^{-1} (O—H and N-H stretching) to 3457 cm^{-1} and its narrowing. The bands associated with the C—N and C—OH stretching and the acetal bonds were weakened as compared to the Cht/PVA spectrum. Such discrepancies indicate an H-bonding formation between the amine and hydroxyl groups of the polymeric matrix with the FeTMPyP (Lebedeva et al., 2017). Indeed, as previously reported by Lebedeva et al. (2017), a shifting of 10 cm^{-1} at the band related to the O-H and N-H stretching is associated with the presence of H-bonding involving the amine and hydroxyl groups and the organic structure from the porphyrin.

Functional groups present in the polymeric matrix are also capable of chelate the Fe(III) metallic center in the porphyrin structure due to the free electrons from nitrogen and oxygen atoms (Bruller et al., 2015). Such interactions, thereby, promote the immobilization and stabilization of the FeTMPyP in the polymeric matrix (Lebedeva et al., 2017). Also, as clearly observed in Fig. 1a, the characteristics bands of the porphyrin were not observed in the Cht/PVA-FeTMPyP spectrum, which can be due to the small amount of such compound as compared to the polymers (0.1 w/w-%). We hypothesize that the

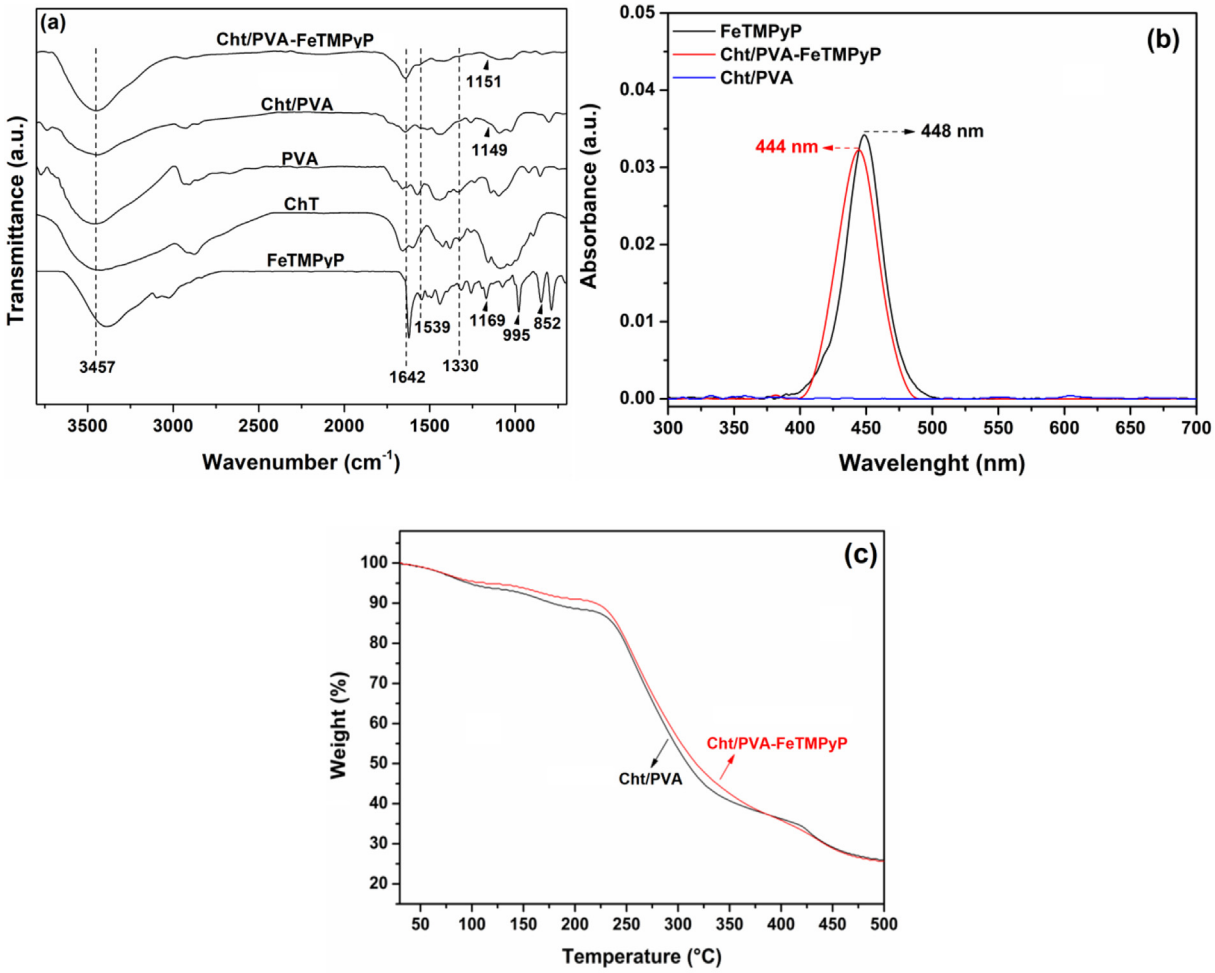

Fig. 1 (a) FTIR spectra of Cht, PVA, FeTMPyP, Cht/PVA film and Cht/PVA-FeTMPyP film, (b) UV–Vis absorption spectra in solid-state of FeTMPyP, Cht/PVA and Cht/PVA-FeTMPyP films and (c) TGA curves of the prepared films.

characteristics bands of FeTMPyP were overlapped by the bands proceeding from Cht and PVA (Synytsya et al., 2009).

UV-Vis measurements in solid-state were also used to characterize the synthesized films and "free" FeTMPyP. The recorded absorption spectra are depicted in Fig. 1b. The FeTMPyP spectrum exhibited a characteristic absorption band in the blue region centered at 448 nm (Soret band). Similarly, the spectrum of the Cht/PVA film embedded with the porphyrin (Cht/PVA-FeTMPyP) exhibited the same Soret band with a slight blue-shifting of ~4 nm likely due to some distortion in the porphyrin core caused by its interaction with the polymeric matrix. As expected, the pristine Cht/PVA film did not show any electronic transition, and for this reason, it does not show absorption in the UV-Vis region. These results confirm the success of the FeTMPyP immobilization into the polymeric film.

TGA and DTG analyses were employed to investigate the thermal properties of Cht/PVA and Cht/PVA-FeTMPyP films. The TGA curves of both films (Fig. 1c) showed four main stages of weight loss. For the Cht/PVA film, the first weight loss (~9% of weight loss) occurred in a temperature range of 30–118 °C, and it can be assigned to the moisture evaporation. The second stage with roughly 12% weighting loss at 167 °C maximum temperature, is attributed to the elimination of the hydroxyl side groups from the PVA chains. The third weight-loss stage (~62% of weight loss), which showed a maximum at 265 °C, is assigned to the thermal degradation of the Cht chains. Finally, the last loss stage (~74% of weight loss) showed a maximum at 434 °C, and it is associated with the degradation of the polyene backbone of PVA. As compared to the Cht/PVA film, the thermal degradation stages of the Cht/PVA-FeTMPyP film occurred in lower temperatures ranges (see DTG data, Fig. S2), likely due to the immobilization of the FeTMPyP in the film matrix. As reported by other authors, the catalytic nature of the FeTMPyP decreases the activation energy of each degradation stage and, thereby, the thermal degradation of the hybrid film is facilitated (Berijani et al., 2018; Sah et al., 2018; Sonkar et al., 2017).

To investigate the influence of the FeTMPyP on the kinetics of thermal degradation of Cht/PVA-FeTMPyP film, we utilized the Arrhenius' equation (Eq. (2)), which is expressed as follows (Bu et al., 2016):

$$k(T) = Ae^{-\frac{E_a}{RT}} \quad (2)$$

where E_a is the activation energy (kJ/mol), A is the frequency factor (1/s), R is the ideal gas constant (8.314 J/mol K), T is the temperature (K), and $k(T)$ is the temperature-dependent

reaction rate constant. This equation can be used to obtain Eq. (3) (see Supplementary material) that correlates the mass loss of the sample (described by α) at a temperature T (Bu et al., 2016).

$$\ln\left(f(\alpha, T)\right) = \ln\left(\frac{AR}{\beta E_a}\right) - \frac{E_a}{RT} \quad (3)$$

Linearization of $f(\alpha,T)$ following an appropriate value of n (1, 2, 3, …) results in E_a estimated from the plot slope. In this work, the kinetic models of first (n = 1), second (n = 2) and third (n = 3) orders were investigated. Overall, the models of second and third orders do not represent the thermal degradation of the polymeric films due to the lower values of the coefficient of determination (R^2) obtained for these kinetic models (data not shown). In contrast, thermal degradation processes for the Cht/PVA and Cht/PVA-FeTMPyP films seem to follow a global first-order reaction mechanism due to the higher R^2 value (data not shown). The estimated values of E_a for each stage of thermal degradation are listed in Table S1.

Overall, the Cht/PVA-FeTMPyP film exhibited lower values of E_a for all thermal degradation stages when compared to the Cht/PVA film confirming that the porphyrin impairs the thermal stability of the polymeric matrix (Table S1). Metalloporphyrins plays a catalytic role in the thermal degradation of polymer-based materials due to the capacity of the metalloporphyrin to enhance the formation of radical species. Then, since the depolymerization reaction of polymeric materials is based on the formation and action of radical species until the complete oxidation, the presence of the metalloporphyrins increases the presence and activity of these species into the polymeric matrix. As a result, the entire degradation process of the hybrid film is facilitated (Huang et al., 2017; Nichols et al., 2018), Moreover, since the first-order mechanism was the model that better fitted the experimental data, it could be inferred that the generation of radical species in the film during its thermal degradation is fast due to the catalysis ascribed to by the immobilized FeTMPyP (Moussout et al., 2016).

SEM images taken of the Cht/PVA and Cht/PVA-FeTMPyP films were used to examine their morphology. The surface of the Cht/PVA film (Fig. S3a) exhibited a smooth and homogenous morphology, which indicates that there is not a phase separation in the film due to the compatibility between the Cht and PVA. Similarly, the SEM image (Fig. S3b), taken from the surface of Cht/PVA-FeTMPyP film, suggests that the hybrid film is also homogeneous. The immobilization of the porphyrin in the polymeric matrix did not promote noticeable changes in the morphology of the film surface. It is worth mentioning that the presence of iron on the Cht/PVA-FeTMPyP film surface was confirmed by EDX elemental analysis (Fig. S3b). The overall picture that emerges from these data suggests that the porphyrin is homogeneously distributed through the polymeric matrix. Also, it does not harm the compatibility between the polymers (i.e., Cht and PVA). The data collected from the previous analysis suggested that FeTMPyP interacts with the polymers chains, mainly by H-bonds, which may enhance its dispersion through the material (de Souza et al., 2017). It should be mentioned that the presence of some marks on the surface of the Cht/PVA-FeTMPyP film is due to slots in the Petri dish utilized as mold.

AFM microscopy was also used to evaluate Cht/PVA and Cht/PVA-FeTMPyP films. This technique provides much more accurate information on the topographic roughness and other surface properties of the samples. AFM images of Cht/PVA and Cht/PVA-FeTMPyP films are shown in Fig. 2. This highly sensitive imaging technique with atomic resolution allowed us to observe that the Cht/PVA-FeTMPyP film presented a much more complex surface than the Cht/PVA film. Although the average roughness (R_a) for both samples is roughly very similar, the fractal dimensions (D) have significant differences. For Cht/PVA film the parameters calculated were R_a = 6.285 and D = 2.214. On the other hand, for Cht/PVA-FeTMPyP film, the AFM images resulted in a R_a = 6.638 and D = 2.262. Both parameters are related with the heterogeneity and irregularity of the sample (Singh et al., 2016), but the fractal dimension, which is a measurement how complex the surface is, when increased by only 10%, can decrease surface stiffness by more than one order of magnitude and can affect many other mechanical properties and modify the area of contact at interfaces (Buzio et al., 2003). As demonstrated by FTIR and TGA analyses, the immobilized porphyrin interacts with the functional groups available in the polymer matrix. Such interactions could promote the formation of FeTMPyP bonded centers with the Cht and PVA chains. These centers must form irregular structures through the polymeric matrix, thereby increasing the irregularity of the film surface (Yivlialin et al., 2017). Finally, the electric force images that are presented with the AFM topography scans show that the Cht/PVA-FeTMPyP film has abundant negative domains dispersed along its surface.

The swelling ability of solid supports embedded with metal species plays a key role in catalytic reactions performed in water. Swellable catalysts assure the access for the reactants to the metal species enhancing the reaction efficiency. Herein, swelling experiments were performed to investigate the liquid uptake capacity of the Cht/PVA and Cht/PVA-FeTMPyP films under different pH conditions. The collected data are presented and discussed in the Supplementary material section (Fig. S5).

3.2. Dye decolorization

Fenton process is among the most representative and efficient AOP techniques, which makes use of Fe(II) (classic Fenton reaction) or Fe(III) (Fenton-like reaction) ions. Overall, these ions catalyze the decomposition of H_2O_2, resulting in different radical species (Eqs. (4)–(7)) that decolorize and degrade organic compounds, such as azo dyes, due to their oxidative ability (Huang et al., 2013). From a practical viewpoint, some studies have indicated that the H_2O_2 decomposition rate is usually slower for reactions catalyzed by Fe(III) ions as compared to Fe(II) ions, which may affect the efficiency of the oxidation reactions. This discrepancy regarding the H_2O_2 decomposition rate is caused by an additional step in the Fenton-like processes related to the gradual conversion of the Fe(III) to Fe(II) ions (Eqs. (6) and (7)).

$$\mathrm{Fe(II)} + \mathrm{H_2O_2} \rightarrow \mathrm{Fe(III)} + \cdot\mathrm{OH} + \mathrm{OH^-} \quad k = 76\ \mathrm{L/mol\ s} \quad (4)$$

$$\mathrm{Fe(III)} + \mathrm{H_2O_2} \rightleftharpoons [\mathrm{Fe(II)(O_2H)}]^{2+} + \mathrm{H^+} \quad K_a = 3.1 \times 10^{-3} \quad (5)$$

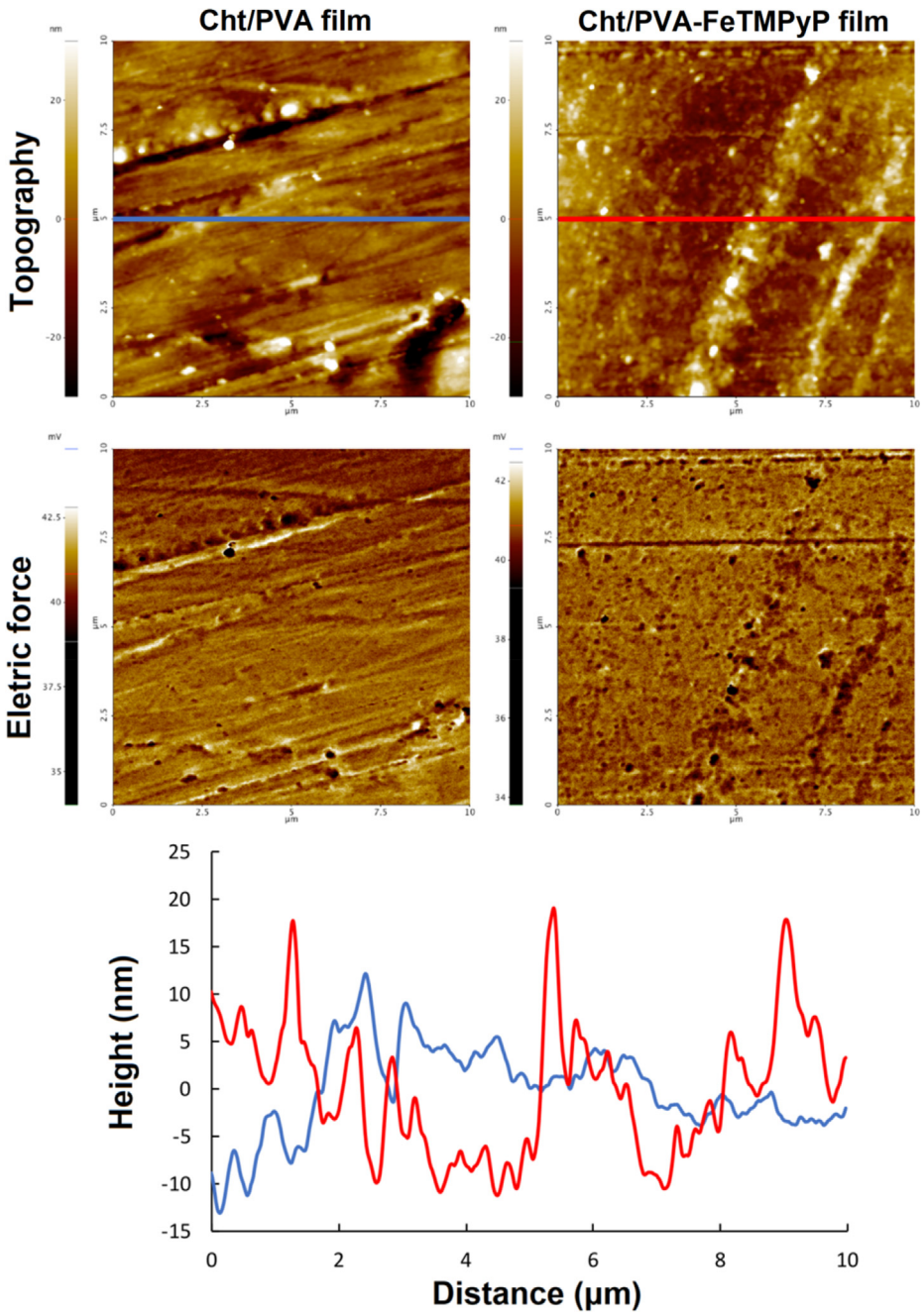

Fig. 2 Topography and electric force images obtained by AFM on Cht/PVA and Cht/PVA-FeTMPyP films. The topography linescans are presented at the bottom.

$$[Fe(II)(O_2H)]^{2+} \rightarrow Fe(II) + {\cdot}O_2H \quad k = 2.7 \times 10^{-3}\ \text{L/mol s} \tag{6}$$

$$Fe(III) + {\cdot}O_2H \rightarrow Fe(II) + H^+ + O_2 \quad k = 1.0 \times 10^{3}\ \text{L/mol s} \tag{7}$$

To overcome this discrepancy associated with the efficiency of Fe(III) ions, porphyrins have been used as organic chelating ligands. These ligands are capable of chelate the Fe(III) ions accelerating their conversion to Fe(II) ions in the presence of H_2O_2, which enhances the efficiency of the Fenton-like processes. Since the overall Fenton reaction is cyclic, the Fe(III) ions are regenerated at the end of the reaction (Wei et al., 2019). Despite the benefits of using porphyrins, in practical situations, they may dissolve in the treated water hampering their recovery and recyclability. Then, in this study, the porphyrin was immobilized into the Cht/PVA matrix, resulting in a hybrid material.

The catalytic activities of the immobilized FeTMPyP and the "free" FeTMPyP in the decolorization of MO and MR azo dyes were investigated under similar experimental conditions. These experiments were conducted using the Cht/PVA-FeTMPyP film (60 mg, which contains 60 μg of porphyrin) or "free" FeTMPyP (60 μg) as catalysts. According to the

results depicted in Fig. 3, it is notorious that the hybrid film had higher catalytic efficiency than the "free" FeTMPyP to decolorize both azo dyes. As assessed, the maximum decolorization rates of MO and MR by "free" FeTMPyP catalyzed reactions were 70% and 68%, respectively. On the other hand, the reactions conducted in the presence of Cht/PVA-FeTMPyP film achieved a decolorization rate of 100% and 92% for MO and MR. For comparison, decolorization reactions of MO and MR were conducted using the Cht/PVA film as the catalyst. In these cases, no decolorization was observed, suggesting that FeTMPyP has a crucial role in these processes. These experiments allow to conclude that (i) the decolorization of both the azo dyes only happens in the presence of both FeTMPyP and H_2O_2, and (ii) the polymeric matrix plays a leading role in the decolorization process since it enhances the catalytic efficiency of the metalloporphyrin, which agrees with previous studies (Chen et al., 2019; Wang et al. 2014a,b; Wei et al., 2019).

There is a clear improvement regarding the dye decolorization efficiency by using the Cht/PVA-FeTMPyP film as the catalyst, even under the milder conditions used here. Shao et al. (2010) reported the use of a hybrid system consisting of Fe(III) tetra-phenylporphyrin (FeTPP) immobilized in electrospun polystyrene (PS) nanofibers mat to the photocatalysis the decolorization of MO. According to the authors, the maximum decolorization rate was 97.8% after 3 h of reaction. However, this decolorization efficiency was only achieved after the introduction of TiO_2 into the nanofiber mat. Also, the amount of H_2O_2 utilized was 10-folds higher than the amount used in this study. The use of other tetrapyrrole-based macrocyclics immobilized in solid supports has also been investigated for the catalytic (or photocatalytic) decolorization of organic dyes (Ahmed et al., 2017; Li et al., 2018). Comparatively, harsh reaction conditions are utilized as well as more onerous processes are required, which highlights the applicability and efficiency of the Cht/PVA-FeTMPyP film.

The degradation of organic pollutants by the Fenton or Fenton-like reactions is exceptionally efficient, but the mechanisms of these reactions are not fully understood. In particular, the identity of the active intermediates responsible for the oxidation of the organic dye has long been debated (Wang et al., 2017a,b). Recently, some studies reported the presence of Fe (IV) (ferryl) ions species in the reaction medium, besides the mentioned oxygen-based radicals, which also could promote the oxidation of organic molecules (Li et al., 2018). The Fe (IV) ions are mainly formed due to the formation of a complex involving the Fe(II) ions and the H_2O_2 (Eq. (8)), which is subsequently decomposed by a two-electron transfer mechanism generating the Fe(IV) species (Eq. (9)) (Lu et al., 2018). Moreover, the ferryl ions are shorter-lived species and considering an electron-rich environment around the metal ion, as in Cht/PVA-FeTMPyP, provided by the porphyrin structure and the functional groups of the matrix, these iron species are in lower quantity and are not the main oxidant species. Thus, although different oxidants are generated from the H_2O_2 cleavage (e.g., $^{\cdot}OH$, $^{\cdot}O_2H$, $^{\cdot}O_2$, and Fe(IV)), the $^{\cdot}OH$ radicals are still the most reactive species generated by the Fenton and Fenton-like reactions (Lu et al., 2018).

$$Fe(II) + H_2O_2 \rightarrow [Fe(II)(H_2O_2)]^{2+} \quad (8)$$

$$[Fe(H_2O_2)] \rightarrow [Fe(IV)O]^{2+} + H_2O \quad (9)$$

In summary, the decolorization process based on the Fenton-like reaction could be resumed as a global two-step's reaction (Eqs. (10) and (11)) (Chen et al., 2019). Firstly, the H_2O_2 is converted to a radical species (which were generically denoted as $^{\cdot}R$) by its active contact with the iron ion. Then, from this active contact, radical species are generated, whereas the $^{\cdot}OH$ radicals are the most reactive of all oxidants produced. Thus, taking that on account, the $^{\cdot}OH$ radicals can promote the oxidation and decolorization/degradation of organic pollutants, such as the azo dyes (Ahmed et al., 2016). Moreover, in heterogeneous Fenton-like reactions, the $^{\cdot}OH$ radicals are commonly generated on the catalyst surface, and the decolorization process is a surface-mediated process. Considering this, the adsorption of the organic molecule on the catalyst surface is crucial to its decolorization process (Chen et al., 2019).

$$Fenton \rightarrow {}^{\cdot}R \quad (10)$$

$$Dye + {}^{\cdot}OH \rightarrow Products \quad (11)$$

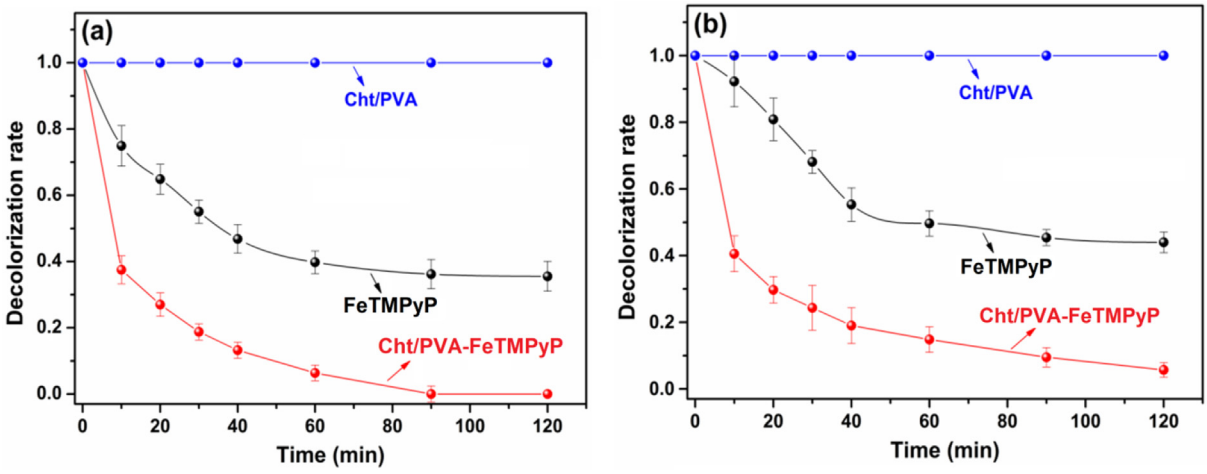

Fig. 3 Catalytic decolorization of (a) MO and (b) MR solutions using "free" FeTMPyP, Cht/PVA film or Cht/PVA-FeTMPyP film (Dye concentration 1 ppm, H_2O_2 concentration 1 mmol/L, room temperature, volume 25 mL, pH 7 and stirring 100 rpm).

As mentioned, the Cht/PVA-FeTMPyP film possesses several functional groups (e.g., amine and hydroxyl groups) distributed along with its matrix, allowing the interaction with the azo dye molecules in solution. This interaction enables the approximation and adsorption of the dye molecules on the film surface. Here, the concentration of MO and MR near the active sites is enhanced, and these "hold" organic molecules are rapidly oxidized by the ·OH radicals, which are generated from the catalytic cleavage of H_2O_2 in the direct neighborhood (Saltarelli et al., 2019). In contrast, without the active polymeric matrix, the H_2O_2 molecules must collide randomly with the FeTMPyP in solution to enable their active contact, and the ·OH radicals are produced. Subsequently, the organic molecules in the solution bulk could be degraded by these oxidant radical species. However, this homogenous process is susceptible to some limitations that could restrict the conversion of the hydrogen peroxide to ·OH radicals impairing the degradation process (Wang et al., 2019).

Indeed, one of the most critical aspects of homogeneous catalysis, considering the use of "free" FeTMPyP, besides a high dispersion and homogeneity, is the stability of the catalyst in the reaction medium. Metalloporphyrins are organic molecules sensitive to reactive oxygen species, and they could be degraded under strong oxidative conditions (Castro et al., 2019). This degradation process consumes ·OH radicals and decreases the availability of FeTMPyP in the reaction medium. These drawbacks affect the generation of ·OH radicals, and hence, the decolorization of the azo dyes is impaired (Lexa et al., 1985). In contrast, the immobilization of the porphyrin into the polymeric matrix enhances its stability while keeps its reactivity (Heydari-Turkmani et al., 2017; Nasrollahi et al., 2019). All these aspects could explain the higher decolorization efficiency presented by the reactions catalyzed by the Cht/PVA-FeTMPyP film as compared to the "free" FeTMPyP.

Moreover, it should be mentioned that the Fenton-like process is susceptible to reaction conditions. Then, the effect of pH, initial dye concentration, H_2O_2 concentration, and catalyst dosage on the decolorization of MO and MR using the Cht/PVA-FeTMPyP film as catalyst was investigated in detail.

3.2.1. Effect of pH

Batch experiments were conducted under different pH conditions to understand the effect of the initial pH on the decolorization of MO and MR. The results are shown in Fig. 4. According to these experiments, it seems that the decolorization of MO and MR is faster under pH conditions higher than 3. Indeed, the decolorization rate of MO achieved 81% and 84% at pH 5 and pH 7 just before 30 min of reaction. Conversely, at pH 3, the decolorization rate of MO was only 75% after this same time interval. Despite this, after 90 min, 100% of the MO solution was decolorized in all tested pH conditions. For the MR, a similar trend was observed (Fig. 4b). At pH 5 and pH 7, after 120 min of reaction, >90% of the MR solution was decolorized, while, at pH 3, the decolorization rate was only 73%. From this experiment, it is evident that the decolorization processes of MO and MR exhibit discrepancies regarding their kinetics, and, in both cases, neutral pH conditions seem to be more efficient than acidic conditions. This last finding contrasts with other previously reported data for the decolorization of azo dyes using the Fenton-like reaction (Yan et al., 2019); meanwhile, it agrees with others (Chen et al., 2019; Huang et al., 2013). In general, the homogenous Fenton-like reaction is efficient only at acid condition, whereas the pH 3 is reported as the better pH condition that provides a higher decolorization efficiency for azo dye solutions (Arshadi et al., 2016). In contrast, the heterogeneous Fenton-like reaction could be applied to a broader pH range and still maintain a high decolorization efficiency (Huang et al., 2013).

Although the exact mechanism of the Fenton-like reaction is still a matter of debate, its efficiency is clearly related to the oxidative power of ·OH radicals. However, during the catalytic cleave of the H_2O_2, other radical species are also generated. These species possess a crucial effect in the Fe(III)/Fe(II) cycle that naturally occurs in the Fenton-like reaction. This cycle is mainly affected by the hydroperoxyl ($^{\cdot}O_2H$) and superoxyl ($^{\cdot}O_2$) radicals (Bu et al., 2016). Therefore, the faster and enhanced decolorization of the azo dyes solutions at higher pH conditions can be explained considering the role

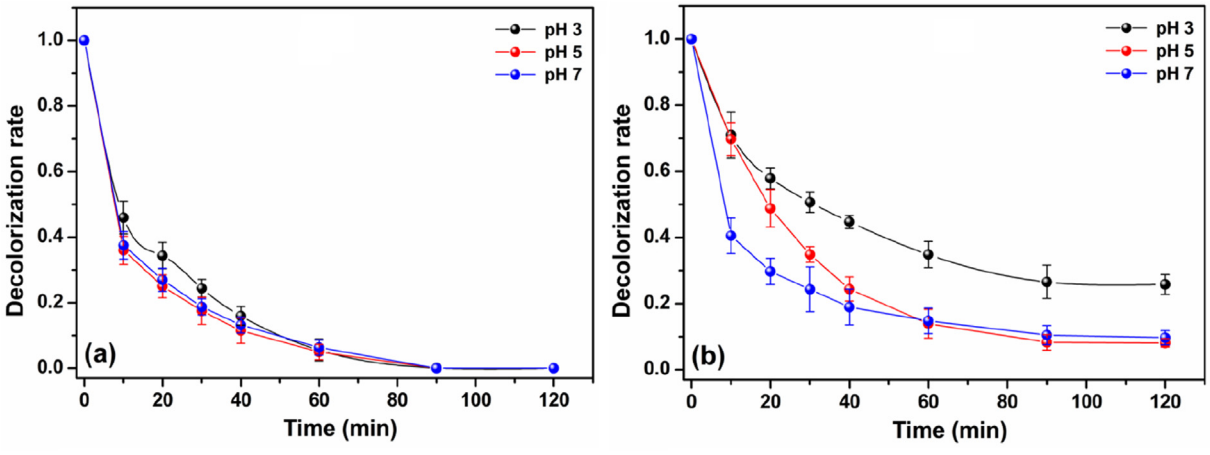

Fig. 4 Effect of pH on decolorization rate of (a) MO and (b) MR using the Cht/PVA-FeTMPyP film (Catalyst dosage 60 mg, dye concentration 1 ppm, H_2O_2 concentration 1 mmol/L, room temperature, volume 25 mL and stirring 100 rpm).

of the $^{\cdot}O_2H/^{\cdot}O_2$ on the Fe(III)/Fe(II), which is summarized by the Eqs. (12)–(16) (Huang et al., 2013). In these equations, the organic ligands of the iron porphyrin were omitted to simplify the explanation (Huang et al., 2013).

$$[Fe(II)]^{2+} + {}^{\cdot}O_2H \rightarrow [Fe(III)(O_2H)]^{2+} \quad k = 1.2 \times 10^6 \text{ L/mol s} \tag{12}$$

$$[Fe(II)]^{2+} + {}^{\cdot}O_2 + H_2O \rightarrow [Fe(III)(O_2H)]^{2+} + OH^- \quad k = 1.0 \times 10^7 \text{ L/mol s} \tag{13}$$

$$Fe(III) + {}^{\cdot}O_2H \rightarrow Fe(II) + O_2 + H^+ \quad k < 1.0 \times 10^3 \text{ L/mol s} \tag{14}$$

$$Fe(III) + {}^{\cdot}O_2 \rightarrow Fe(II) + O_2 \quad k = 5.0 \times 10^7 \text{ L/mol s} \tag{15}$$

$$^{\cdot}O_2H \rightleftharpoons H^+ + {}^{\cdot}O_2 \quad pK_a = 4.88 \tag{16}$$

The Eqs. (12)-(16) shown that both $^{\cdot}O_2H$ and $^{\cdot}O_2$ are essential for the cyclic conversion involving the Fe(III) and Fe(II) ions. Thereby, according to these set of equations, at pH < 4.88, the $^{\cdot}O_2H$ radical exists in excess (Eq. (16)) and, as a result, the equilibrium shifts to the formation of Fe(III) (Eq. (13)) rather than to Fe(II), (Eq. (14)) since the conversion for the ferrous ions is faster (see the described kinetic constants for these reactions). At higher pH conditions (pH > 4.88), the $^{\cdot}O_2H$ radicals are easily decomposed to $^{\cdot}O_2$ radicals, as demonstrated by Eq. (16). In the presence of an excess of $^{\cdot}O_2$, the equilibrium is displaced to the formation of Fe(II) (Eqs. (13) and (15)). Then, the conversion of Fe(III) to Fe(II) by the $^{\cdot}O_2$ radicals (Eq. (15)) is the rate-limiting step at a higher pH condition (pH ≥ 5). Thus, the pH plays a crucial role in the Fe(III)/Fe(II) cycle and could accelerate the reduction of Fe (III) to Fe(II) and enhance its half-life in the reaction. As a result, more $^{\cdot}OH$ radicals are generated, and a higher number of azo dyes molecules can be decolorized (Huang et al., 2013). Further, the expansion of the polymeric matrix is limited under neutral pH conditions, and the generation of $^{\cdot}OH$ radicals is restricted on the Cht/PVA-FeTMPyP film surface, which increases and facilitates their contact with the dye molecules. On the other hand, at pH 3 the polymeric matrix can expand due to the cation-cation repulsion forces between the protonated amine and hydroxyl groups, and the FeTMPyP could be release and degraded by the strong oxidative species in the reaction medium. Hence, the decolorization process of the azo dyes it would inevitably be hampered. After these experiments, the film samples were recovered and analyzed by UV-Vis measurements (Figs. S6 and S7). In fact, the post-utilized samples still possess the characteristic absorption band of FeTMPyP, which indicates the stability of the immobilized porphyrin even after the experiments. It is worth mentioning that these samples still maintained their weight, color, and did not become brittle after these reactions. Finally, considering these results, further Fenton-like reactions were performed at pH 7.

3.2.2. *Effect of initial MO and MR concentration*

The decolorization of MO and MR solutions was also studied by changing the initial concentration of the azo dyes while maintaining other experimental conditions invariable. The results are presented in Fig. 5a and 5b. Overall, it seems that the decolorization process is favorable at lower dye concentrations for both azo dyes tested. For the MO, the decolorization rate at 1 ppm of MO increased quickly and achieved 90% before 40 min of reaction. At this same time interval, an increase of MO concentration to 10 ppm and 20 ppm reduced the decolorization rate to 84% and 79%, respectively. After 120 min of reaction, >98% of the MO was degraded independently of its initial concentration in solution. The decolorization of the MR solution also presented this same trend, although it was more pronounced. For the MR, after 120 min, the decolorization rate achieved 92%, 85%, and 81% at the initial MR concentrations of 1, 10, and 20 ppm, respectively. Despite the high decolorization rates achieved at high initial concentrations of both dyes (>80%), the decrease of efficiency as compared to the lowest initial concentration can be explained by the limited amount of $^{\cdot}OH$ radicals in the reaction medium compared to the number of dye molecules, which increases considerably at high MO and MR concentrations ([*Dye*] ≫ [$^{\cdot}OH$]). Under these experimental conditions, the amount of $^{\cdot}OH$ radicals generated is

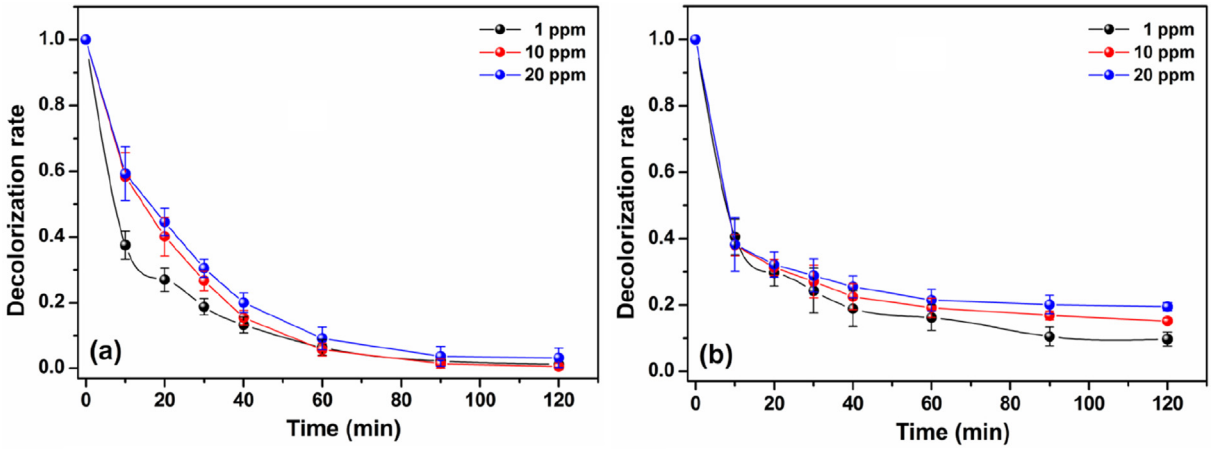

Fig. 5 Effect of initial dye concentration on decolorization rate of (a) MO and (b) MR using the Cht/PVA-FeTMPyP film (Catalyst dosage 60 mg, H_2O_2 concentration 1 mmol/L, room temperature, volume 25 mL, pH 7 and stirring 100 rpm).

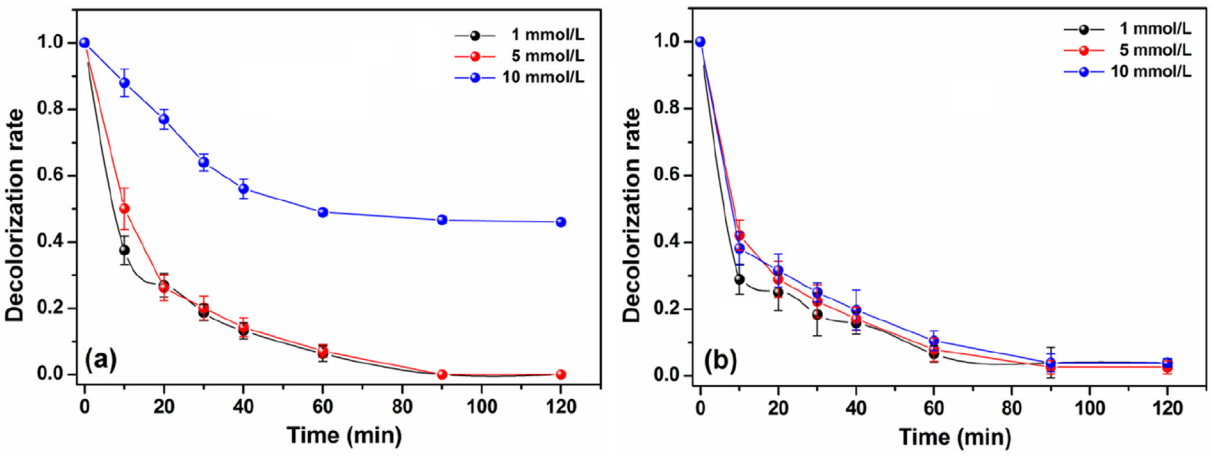

Fig. 6 Effect of H_2O_2 concentration on decolorization rate of (a) MO and (b) MR using the Cht/PVA-FeTMPyP film (Catalyst dosage 60 mg, dye concentration 1 ppm, room temperature, volume 25 mL, pH 7 and stirring 100 rpm).

insufficient to promote a fast decolorization of the dye molecules (Nasrollahi et al., 2019).

3.2.3. *Effect of H_2O_2 concentration*

The effect of H_2O_2 concentration on the decolorization of MO and MR by the Fenton-like process is shown in Fig. 6. According to the experimental results, it was observed that the decolorization of both azo dyes is more efficient at low H_2O_2 concentrations (1 and 5 mmol/L). In parallel, the decolorization of the MO and MR solutions showed to be less effective when a high H_2O_2 concentration (10 mmol/L) is utilized. This effect seems to be more evident for the MO decolorization process, where only 55% of MO was decolorized after 120 min of reaction when the H_2O_2 concentration was set to 10 mmol/L (Fig. 6a). On the other hand, low H_2O_2 concentrations ($\leq$5 mmol/L) assured a complete decolorization of the MO solution at the end of the experiment. Accordingly to the results shown in Fig. 6b, changes in the H_2O_2 concentration caused a slight variation in the MR decolorization process. Anyway, MR solution as faster decolorized at the lowest H_2O_2 concentration (1 mmol/L). Usually, a scavenging effect toward the $^{\cdot}OH$ radicals generated during the Fenton reaction occurs when high H_2O_2 concentrations are utilized. As a result, $^{\cdot}O_2H$ radicals are generated in the reaction media (Eq. (17)). The $^{\cdot}O_2H$ radicals exhibit an attenuated oxidative ability and can also scavenge the $^{\cdot}OH$ radicals (Eq. (18)) (Ahmed et al., 2016; Huang et al., 2013). In general, these harmfully side reactions decrease the amount of $^{\cdot}OH$ radicals that could attack the dyes molecules and, consequently, the decolorization process is harmed. Additionally, solid-state UV–Vis measurements performed with the post-utilized film samples showed that the immobilized FeTMPyP was not degraded by the strong oxidative medium (Figs. S8 and S9). These results confirm the stability of the immobilized porphyrin likely due to its interaction with the polymeric matrix.

$$H_2O_2 + {}^{\cdot}OH \rightarrow H_2O + {}^{\cdot}O_2H \quad (17)$$

$$^{\cdot}O_2H + {}^{\cdot}OH \rightarrow H_2O + O_2 \quad (18)$$

Considering that the decolorization of both azo dye solutions using 1 mmol/L of H_2O_2 was efficient, this concentration was set as the optimum concentration for the Fenton-like process.

3.2.4. *Effect of catalyst dosage*

The decolorization of azo dye solutions by Fenton-like processes is also dependent on the catalyst dosage. Thus, the effect of the catalyst dosage on the decolorization of MO and MR was investigated by varying the mass of the Cht/PVA-FeTMPyP film. Herein, three different catalysts masses were tested; 60, 80, and 100 mg. In these samples, the amount of FeTMPyP immobilized in each one represents 0.1 w/w-% of the total mass. The data collected from these sets of experiments are shown in Fig. 7. In general lines, the decolorization kinetics of the MO solution increased when the catalyst dosage increased from 60 to 100 mg (Fig. 7a). However, after 90 min of reaction, 100% of the MO solution was decolorized independently of the catalyst dosage. The increment in the decolorization kinetics noticed for the reactions conducted with high catalyst dosages can be associated with the increase of active sites on the film surface, which generates more $^{\cdot}OH$ radicals. Consequently, the higher availability of radicals speeds out the decolorization of the MO solution (Ahmed et al., 2016). Conversely, the effect of the catalyst dosage on the decolorization of the MR solution was negligible until the first 60 min of reaction (Fig. 7b). After this while, the decolorization rate increased as decreased catalyst dosage. At the end of the experiment, the decolorization rate achieved 92%, 88%, and 84% using 60 mg, 80 mg, and 100 mg of the catalyst. To note, the decolorization rate remains constant for all tested catalyst dosages after 90 min of reaction, which indicates that the overall decolorization process ceased.

This discrepant behavior presented by the MR, in comparison with the MO, is not usual since the unique difference between the performed decolorization systems is the dye used. Moreover, the only molecular distinction between MR and MO is the presence of a carboxyl group instead of a sulfonate group. According to the literature, the MR molecule is more resistant to oxidative action and, thereby, its decolorization

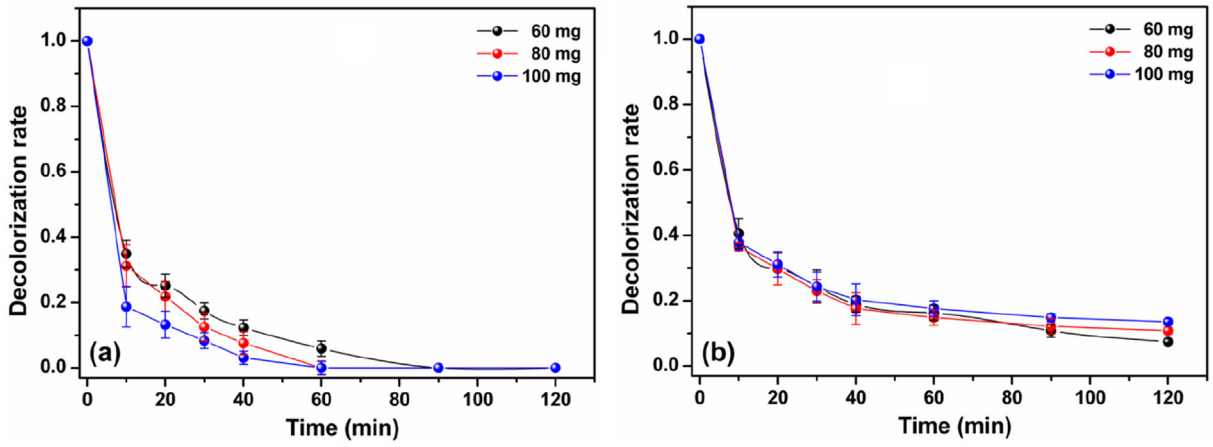

Fig. 7 Effect of catalyst dosage on decolorization rate of (a) MO and (b) MR using the Cht/PVA-FeTMPyP film (Dye concentration 1 ppm, H_2O_2 concentration 1 mmol/L, room temperature, volume 25 mL, pH 7 and stirring 100 rpm).

by the Fenton-like processes is harder than the MO (Rufus and Philip, 2016). Besides that, the increase of the catalyst dosage (sample mass) also affects the mass transfer rates of H_2O_2 and MR in the solution bulk that could lead to a decrease in the decolorization efficiency (Fang et al., 2017). Such behavior became extremely important, considering that the MO possesses a higher solubility in water than the MR (Cardona and Magri, 2014). Therefore, the neighborhood iron sites scavenge the surface-generated ·OH radicals due to the lack of adsorbed MR molecules on the film surface (Liang et al., 2012). Thus, the increasing of the catalyst dosage affects negatively the decolorization of MR, which is coherent with our experimental results. In contrast, the higher solubility of MO enhances its adsorption on the film surface, favoring the attack the ·OH radicals. Therefore, the increase in the catalyst dosage enhances the decolorization of the MO solution.

Another experimental finding that should be highlighted here is related to the amount of Fe(III) ions used to decolorize the MO or MR solutions under these experimental conditions. As assessed, high decolorization rates were achieved using 60 mg of the hybrid film, which was embedded with 60 μg of FeTMPyP. More specifically, 60 mg of the hybrid film contains ~ 3.7 μg of Fe(III) ions, which is a meager amount when compared to other catalysts used in Fenton-like reactions. These results highlight the viability and employability of this new hybrid film in practical wastewater contaminated by azo dyes.

3.3. Kinetics of decolorization

Further experiments on the decolorization of MO and MR by the heterogeneous Fenton-like system were investigated in detail considering the tested variables (i.e., initial dye concentration, H_2O_2 concentration, and catalyst dosage).

The decolorization of azo dye solutions by the Fenton-like reaction is a complex process; therefore, it is convenient to assume some mechanistic simplifications, mainly regarding the active oxidative species responsible for the degradation and decolorization process. As aforementioned, the ·OH radicals are often considered as the most reactive oxidant species produced by the Fenton-like reaction. Thus, to the kinetic investigation, it was assumed that the decolorization of MO and MR follows an ·OH-mediated mechanism exclusively, as other studies also did (Lu et al., 2018; Wang et al., 2017a,b).

According to this mechanism, the ·OH radicals are produced by the reaction between the H_2O_2 and the catalyst. After that, these radicals attack and degrade the dye molecules (Eqs. (17) and (18)). Then, the rate generation of ·OH is directly related to the catalytic efficiency of the Fenton-like catalyst. In this case, the decolorization of azo dyes solutions is also a surface-mediated process and, thereby, the azo dye adsorption on the catalyst surface is crucial to a high decolorization efficiency. In this sense, the Langmuir-Hinshelwood mechanism is applicable to describe this process since it assumes that the reaction among the ·OH radicals generated on the surface of the catalyst takes place with dye molecules adsorbed on the catalyst surface (Liang et al., 2012). In general, this mechanism is typically fitted by a second-order equation (Eq. (19)) since it depends on the amount of azo dye adsorbed ($[Dye_{ad}]$) and ·OH radicals' concentration ([·OH]) on the catalyst (Liang et al., 2012). Assuming instantaneous adsorption of azo dyes molecules and a steady-state approximation with respect to ·OH radicals, since these radicals are in excess in the medium, the decolorization process can be simplified to the pseudo-first-order equation, which is often described as Eq. (20) (Quadrado and Fajardo, 2017).

$$\frac{dA}{dt} = -k[Dye_{ad}][\,^{\cdot}OH] \tag{19}$$

$$ln\left(\frac{A_0}{A_t}\right) = k_{app}t \tag{20}$$

Eq. (20) is the linearized form of the pseudo-first-order kinetics, where A_o and A_t are the absorbance of azo dyes solutions at the initial time ($t = 0$) and reaction time ($t \neq 0$), k_{app} (1/min) is the pseudo-first-order apparent rate constant, and t (min) is the time. The k_{app} constant can be calculated from the slope of the linear plot of $\ln(A_o/A_t)$ as a function of t (Figs. S5-S7). The calculated k_{app} values, as well as the determination parameters (R^2) and the half-time ($t_{1/2}$) values for the decolorization of MO and MR at different experimental conditions, are reported in Table S2. It is worth to inform

that zero-order and pseudo-second-order kinetics were also investigated (Ali et al., 2013). Such models presented lower R^2 values for both azo dyes in all tested conditions (data not shown), indicating that they were not adequate to explain the experimental data.

The decolorization of both MO and MR solutions by the Fenton-like process using the Cht/PVA-FeTMPyP as catalyst was fitted by the pseudo-first-order kinetic model ($R^2 > 0.97$) (see Table S2). The adequacy of the pseudo-first-order model to the experimental data seems to be a reasonable find. As it was extensively discussed before, in our experimental conditions, the ·OH radicals are in excess, especially in the catalyst surface, due to the equilibrium rebalance reached in neutral to alkaline pH (see Section 3.2.1). Thus, it is possible to consider that the [·OH] is practically invariant during the decolorization reaction of the MO and MR. Such inference is supported by the fast-kinetic degradation rate that happens in a single kinetic stage (Figs. S10–S12). This one-stage kinetics is related to a quick generation of ·OH radicals on the catalyst surface during the whole decolorization process (Liang et al., 2012). Moreover, it also means efficient adsorption of the azo dyes molecules on the catalyst surface (Liang et al., 2012). These finds indicate that the Langmuir-Hinshelwood mechanism takes place in the decolorization of MO and MR by the Fenton-like reaction catalyzed by the Cht/PVA-FeTMPyP film.

The hybrid film developed in this study showed k_{app} constants comparable to or better than other similar catalysts based on stabilized iron ions. Table 1 displays a comparative chart of the decolorization efficiency of MO and MR using different Fenton and Fenton-like catalysts. As noticed, the Cht/PVA-FeTMPyP film showed a high decolorization efficiency towards the decolorization of both azo dyes, even using low amounts of H_2O_2 (1 mmol/L), catalyst (60 mg) and mild experimental conditions (pH ≈ 7 and room temperature). All these features rank the Cht/PVA-FeTMPyP film as a promising material for practical uses.

3.4. Decolorization process mechanism

Considering all the previously discussed aspects of the decolorization of the MO and MR solutions and the role of each component of both systems, the Fig. 8 summarizes a simple proposed mechanism for the decolorization process (Kakavandi and Babaei, 2016). In summary, the ·OH radicals, generated on the catalyst surface due to the catalytic cleave of H_2O_2 by the immobilized FeTMPyP, attack the adsorbed dyes molecules in the direct vicinity of the active sites. These ·OH radicals promote the structural degradation of MO and MR molecules by attacking their azo bonds (—N=N—) that are closely related to the color characteristic in solution. So, the decolorization of an azo dye solution indicates the structural degradation of dye molecules to the simplest compounds (Kakavandi and Babaei, 2016).

The by-products generated from the decolorization reactions were isolated from the reaction media and analyzed by FTIR and GC-MS. The obtained data are presented and discussed in the Supplementary material file (Figs. S14 and S15).

3.5. Reusability

The reusability of the Cht/PVA-FeTMPyP film as the catalyst in the MO and MR decolorization reaction was investigated in consecutive runs using a unique film sample. Overall, the catalytic efficiency of the hybrid film is maintained for at least five consecutive decolorization reactions, as shown in Fig. 9. Overall, the decolorization rates remained higher than 95% for both MO and MR solutions (see Fig. 9). Also, SEM images (Fig. S17) taken from the post-utilized Cht/PVA-FeTMPyP films utilized in the decolorization of MO and MR revealed

Table 1 Efficiency of different Fenton and Fenton-like catalysts on the decolorization of MO and MR under optimal conditions.

Catalyst	Dye	Dye conc. (ppm)	pH	H_2O_2 conc. (mol/L)	Reaction time (min)	Decolorization efficiency	Ref.
Alginate-Fe^{2+}	MO	20	3	1×10^{-3}	30	98%	(Quadrado and Fajardo, 2017)
Alginate-Fe^{3+}	MO	20	3	1×10^{-3}	30	98%	(Quadrado and Fajardo, 2017)
Mesoporous Fe_2O_3-SiO_2	MO	600	2.93	25.1	20	90%	(Panda et al., 2011)
Steel industry waste	MO	20	2	34×10^{-3}	30	98%	(Ali et al., 2013)
Fe_2GeS_4 nanoparticles	MO	20	7	50×10^{-3}	10	100%	(Shi et al., 2018)
Si/Al@Fe/MWCNT	MO	5	4	30	6	89%	(Arshadi et al., 2016)
Fe_2MnO_4 activated carbon	MO	50	4	18×10^{-3}	120	100%	(Thi, et al., 2011)
Fe_3O_4 nanoparticles	MO	20	2	0.64	20	99%	(Jia et al., 2019)
"free" FeTMPyP	MO	10	7	1×10^{-3}	120	70%	*this work*
Cht/PVA-FeTMPyP	MO	10	7	1×10^{-3}	90	100%	*this work*
Fenton's reagent	MR	13.5	< 2	1	2	42%	(Ashraf et al., 2006)
Hydroxysulphate green rust	MR	3	7	1×10^{-2}	60	100%	(Kone et al., 2009)
Fe_3O_4 nanoparticles	MR	50	7	1×10^{-1}	60	50%	(Solomon et al., 2012)
"free" FeTMPyP	MR	10	7	1×10^{-3}	120	68%	*this work*
Cht/PVA-FeTMPyP	MR	10	7	1×10^{-3}	90	100%	*this work*

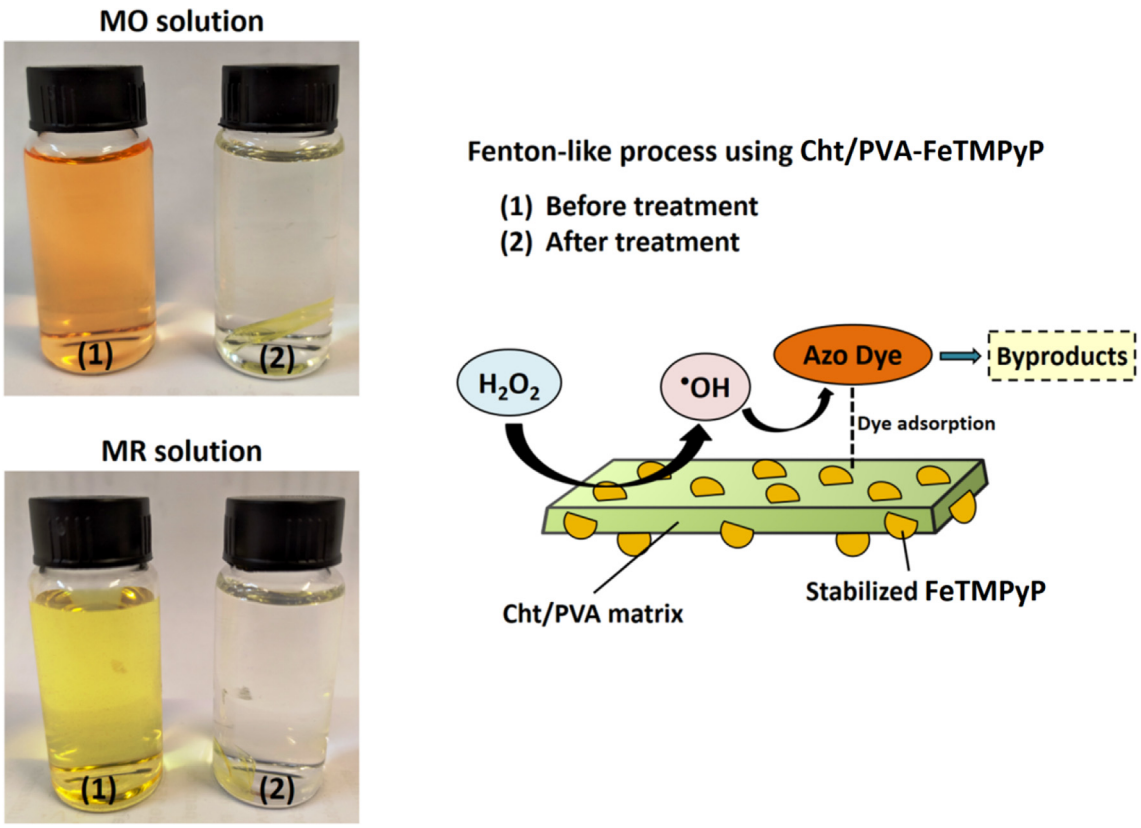

Fig. 8 Illustrative scheme of the azo dye degradation catalyzed by Cht/PVA-FeTMPyP film.

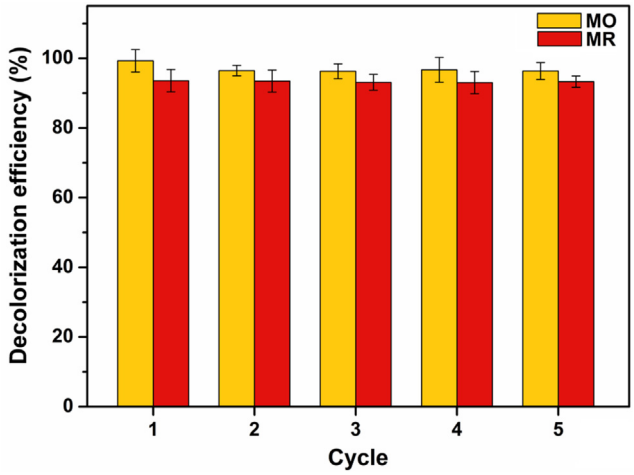

Fig. 9 Efficiency of Cht/PVA-FeTMPyP film on consecutive MO and MR decolorization reactions (Catalyst dosage 60 mg, dye concentration 1 ppm, H_2O_2 concentration 1 mmol/L, room temperature, volume 25 mL, reaction time 90 min, pH 7 and stirring 100 rpm).

slight changes on the surfaces of the catalysts after the reuse cycles. In addition, the film sample showed a negligible mass loss after the reuse cycles (~0.05%, considering the initial and the final mass of the sample at the end of the experiments), and did not become brittle, indicating high film stability.

EDX and solid-state UV-Vis analyses of the post-utilized catalysts indicate that the amounts of FeTMPyP leached after the consecutive decolorization reactions are negligible (Figs. S18 and S19). The maintenance of the decolorization efficiency and the overall stability of the Cht/PVA-Fe(III) film allow indicates that it is a promising material to act as a heterogeneous catalyst in Fenton-like reactions. It should also be highlighted the easy handling of this hybrid film, which can be added and recovery from the reaction medium with tweezers, which stands out that neither sophisticated methods or onerous process (e.g., filtration, magnetic recovery, centrifugation, among others) are needed.

4. Conclusions

Cationic Fe(III)-porphyrin (FeTMPyP) was efficiently immobilized in a chitosan/poly(vinyl alcohol) (Cht/PVA) polymeric matrix resulting in a hybrid material, which was tested as a catalyst in heterogeneous Fenton-like reaction for decolorization of two selected azo dyes (methyl orange, MO, and methyl red, MR) in water. Data collected from characterization analysis revealed that the porphyrin affected the final properties of the hybrid film as compared to the pristine film likely due to the interaction between the porphyrin and the polymeric matrix. Such interaction is beneficial to the immobilization and promotes a good dispersion of the porphyrin through the film. Batch experiments indicated that the immobilization of the FeTMPyP in the Cht/PVA film enhances its catalytic activity towards the decolorization of both azo dyes in the

presence of H_2O_2. Furthermore, both MO and MR solutions were decolorized quickly by heterogeneous Fenton-like reactions using low amounts of the catalyst and H_2O_2. Also, mild experimental conditions (pH 7 and room temperature) were utilized, which is an advantage as compared to other similar studies reported in the literature. As assessed, the decolorization processes followed pseudo-first-order kinetics, while their mechanism can be explained based on the Langmuir-Hinshelwood model. Reuse experiments showed that the Cht/PVA-FeTMPyP hybrid film keeps its catalytic activity for at least 5 consecutive reaction runs without losing efficiency or leach out the iron immobilized in its matrix.

Declarations of interest

The authors declare that they have no known competing financial interests or personal relationships that could have appeared to influence the work reported in this paper.

Acknowledgements

The authors thank to CNPq for their financial support (Universal grant. - Processes 404744/2018-4 and 409150/2018-5). CNPq is also acknowledged for the PQ fellowships to A.R.F. and B.A.I. (Processes 303872/2019-5 and 304711/2018-7). This study was financed in part by the Coordenação de Aperfeiçoamento de Pessoal de Nível Superior, Brazil (CAPES/Proap and Proex) Finance Code 001 and MCT/Finep/CT-Infra 02/2010.

Appendix A. Supplementary material

Supplementary data to this article can be found online at https://doi.org/10.1016/j.arabjc.2020.04.021.

References

Ahmed, M.A., Abou-Gamra, Z.M., Medien, H.A.A., Hamza, M.A., 2017. Effect of porphyrin on photocatalytic activity of TiO_2 nanoparticles toward Rhodamine B photodegradation. J. Photochem. Photobi. B 176, 25–35.

Ahmed, Y., Yaakob, Z., Akhtar, P., 2016. Degradation and mineralization of methylene blue using a heterogeneous photo-Fenton catalyst under visible and solar light irradiation. Cat. Sci. Tech. 6 (4), 1222–1232.

Ali, M.E.M., Gad-Allah, T.A., Badawy, M.I., 2013. Heterogeneous Fenton process using steel industry wastes for methyl orange degradation. Appl. Water Sci. 3, 1–7.

Arshadi, M., Abdolmaleki, M.K., Mousavinia, F., Khalafi-Nezhad, A., Firouzabadi, H., Gil, A., 2016. Degradation of methyl orange by heterogeneous Fenton-like oxidation on a nano-organometallic compound in the presence of multi-walled carbon nanotubes. Chem. Eng. Res. Design 112, 113–121.

Ashraf, S.S., Rauf, M.A., Alhadrami, S., 2006. Degradation of Methyl Red using Fenton's reagent and the effect of various salts. Dye Pigment 69 (1–2), 74–78.

Berijani, K., Farokhi, A., Hosseini-Monfared, H., Janiak, C., 2018. Enhanced enantioselective oxidation of olefins catalyzed by Mn-porphyrin immobilized on graphene oxide. Tetrahedron 74 (18), 2202–2210.

Berradi, M., Hsissou, R., Khudhair, M., Assouag, M., Cherkaoui, O., El Bachiri, A., El Harfi, A., 2019. Textile finishing dyes and their impact on aquatic environs. Heliyon 5 (11), e02711.

Bruller, S., Liang, H.W., Kramm, U.I., Krumpfer, J.W., Feng, X.L., Mullen, K., 2015. Bimetallic porous porphyrin polymer-derived non-precious metal electrocatalysts for oxygen reduction reactions. J. Mater. Chem. A 3 (47), 23799–23808.

Bu, Q., Lei, H.W., Qian, M., Yadavalli, G., 2016. A thermal behavior and kinetics study of the catalytic pyrolysis of lignin. RSC Adv. 6 (103), 100700–100707.

Buzio, R., Boragno, C., Biscarini, F., De Mongeot, F.B., Valbusa, U., 2003. The contact mechanics of fractal surfaces. Nat. Mater. 2 (4), 233–236.

Cardona, M.A., Magri, D.C., 2014. Synthesis and spectrophotometric studies of water-soluble amino bis(ethanesulfonate) azobenzene pH indicators. Tetrahedron Lett. 55 (33), 4559–4563.

Castro, K., Moura, N.M.M., Figueira, F., Ferreira, R.I., Simoes, M. M.Q., Cavaleiro, J.A.S., Neves, M., 2019. New materials based on cationic porphyrins conjugated to chitosan or titanium dioxide: synthesis, characterization and antimicrobial efficacy. Int. J. Mol. Sci. 20 (10), E2522.

Chen, Y.A., Potschke, P., Pionteck, J., Voit, B., Qi, H.S., 2019. Fe_3O_4 nanoparticles grown on cellulose/GO hydrogels as advanced catalytic materials for the heterogeneous fenton-like reaction. ACS Omega 4 (3), 5117–5125.

Chung, K.T., 2016. Azo dyes and human health: A review. J. Environ. Sci. Health C 34 (4), 233–261.

da Silva, G., Pires, S.M.G., Silva, V.L.M., Simoes, M.M.Q., Neves, M., Rebelo, S.L.H., Cavaleiro, J.A.S., 2014. A green and sustainable method for the oxidation of 1,3-dihydrobenzo c thiophenes to sulfones using metalloporphyrin complexes. Cat. Commun. 56, 68–71.

de Souza, J.F., da Silva, G.T., Fajardo, A.R., 2017. Chitosan-based film supported copper nanoparticles: A potential and reusable catalyst for the reduction of aromatic nitro compounds. Carbohyd. Polym. 161, 187–196.

Devi, L.G., Nithya, P.M., 2018. Photocatalytic activity of Hemin (Fe (III) porphyrin) anchored $BaTiO_3$ under the illumination of visible light: synergetic effects of photosensitization, photo-Fenton photocatalysis processes. Inorganic Chemi. Front. 5 (1), 127–138.

Dong, S.Y., Feng, J.L., Fan, M.H., Pi, Y.Q., Hu, L.M., Han, X., Sun, J.H., 2015. Recent developments in heterogeneous photocatalytic water treatment using visible light-responsive photocatalysts: a review. RSC Adv. 5 (19), 14610–14630.

Emmert, F.L., Thomas, J., Hon, B., Gengenbach, A.J., 2008. Metalloporphyrin catalyzed oxidation of methyl yellow and related azo compounds. Inorg. Chim. Acta 361 (8), 2243–2251.

Fang, Z.D., Zhang, K., Liu, J., Fan, J.Y., Zhao, Z.W., 2017. Fenton-like oxidation of azo dye in aqueous solution using magnetic Fe_3O_4-MnO_2 nanocomposites as catalysts. Water Sci. Eng. 10 (4), 326–333.

Gao, W., Tian, J., Fang, Y., Liu, T., Zhang, X., Xu, X., Panel, A., 2020. Visible-light-driven photo-Fenton degradation of organic pollutants by a novel porphyrin-based porous organic polymer at neutral pH. Chemosphere, 243, 125334

Hassan, H., Hameed, B.H., 2011. Oxidative decolorization of Acid Red 1 solutions by Fe-zeolite Y type catalyst. Desalination 276 (1–3), 45–52.

He, Q.G., Mugadza, T., Kang, X.W., Zhu, X.B., Chen, S.W., Kerr, J., Nyokong, T., 2012. Molecular catalysis of the oxygen reduction reaction by iron porphyrin catalysts tethered into Nafion layers: An electrochemical study in solution and a membrane-electrode-assembly study in fuel cells. J. Power Source 216, 67–75.

Heydari-Turkmani, A., Zakavi, S., Nikfarjam, N., 2017. Novel metal free porphyrinic photosensitizers supported on solvent-induced Amberlyst-15 nanoparticles with a porous structure. New J. Chem. 41 (12), 5012–5020.

Holkar, C.R., Jadhav, A.J., Pinjari, D.V., Mahamuni, N.M., Pandit, A.B., 2016. A critical review on textile wastewater treatments: Possible approaches. J. Environ. Manag. 182, 351–366.

Huang, G., Liu, Y., Cai, J.L., Chen, X.F., Zhao, S.K., Guo, Y.A., Li, X., 2017. Heterogeneous biomimetic catalysis using iron porphyrin for cyclohexane oxidation promoted by chitosan. Appl. Surface Sci. 402, 436–443.

Huang, L.Z., Zhu, M.T., Liu, Z.Z., Wang, Z.P., Hansen, H.C.B., 2019. Single sheet iron oxide: An efficient heterogeneous electro-Fenton catalyst at neutral pH. J. Hazard. Mat. 364, 39–47.

Huang, W.Y., Brigante, M., Wu, F., Mousty, C., Hanna, K., Mailhot, G., 2013. Assessment of the Fe(III)-EDDS complex in fenton-like processes: from the radical formation to the degradation of bisphenol A. Environ. Sci. Tech. 47 (4), 1952–1959.

Jia, X.K., Chen, X., Liu, Y., Zhang, B.L., Zhang, H.P., Zhang, Q., 2019. Hydrophilic Fe_3O_4 nanoparticles prepared by ferrocene as high-efficiency heterogeneous Fenton catalyst for the degradation of methyl orange. Appl. Organometal. Chem. 33 (4), 1–8.

Jin, Q.Q., Kang, J., Chen, Q., Shen, J.M., Guo, F., Chen, Z.L., 2020. Efficiently enhanced Fenton-like reaction via Fe complex immobilized on silica particles for catalytic hydrogen peroxide degradation of 2,4-dichlorophenol. Appl Cat. B, 268.

Kakavandi, B., Babaei, A.A., 2016. Heterogeneous Fenton-like oxidation of petrochemical wastewater using a magnetically separable catalyst (MNPs@C): process optimization, reaction kinetics and degradation mechanisms. RSC Adv. 6 (88), 84999–85011.

Kone, T., Hanna, K., Abdelmoula, M., Ruby, C., Carteret, C., 2009. Reductive transformation and mineralization of an azo dye by hydroxysulphate green rust preceding oxidation using H_2O_2 at neutral pH. Chemosphere 75 (2), 212–219.

Kumar, S., Ye, F., Dobretsov, S., Dutta, J., 2019. Chitosan nanocomposite coatings for food, paints, and water treatment applications. Appl. Sci. Basel 9 (12), 2409–2417.

Lebedeva, N.S., Gubarev, Y.A., Yurina, E.S., Smirnova, E.N., Syrbu, S.A., 2017. A new strategy for targeted delivery of non-water-soluble porphyrins in chitosan-albumin capsules. Colloid Polym. Sci. 295 (11), 2173–2182.

Lexa, D., Momenteau, M., Saveant, J.M., Feng, X., 1985. Redox properties and stability of hydroxy complexes of protected iron(III) and iron(II) porphyrins. Inorg. Chem. 24 (2), 122–127.

Li, Y.J., Wang, L.M., Gao, Y., Yang, W.J., Li, Y.Y., Guo, C.C., 2018. Porous metalloporphyrinic nanospheres constructed from metal 5,10,15,20-tetraksi(4 '-ethynylphenyl)porphyrin for efficient catalytic degradation of organic dyes. RSC Adv. 8 (14), 7330–7339.

Liang, X.L., Zhong, Y.H., He, H.P., Yuan, P., Zhu, J.X., Zhu, S.Y., Jiang, Z., 2012. The application of chromium substituted magnetite as heterogeneous Fenton catalyst for the degradation of aqueous cationic and anionic dyes. Chem. Eng. J. 191, 177–184.

Lu, H.F., Chen, H.F., Kao, C.L., Chao, I., Chen, H.Y., 2018. A computational study of the Fenton reaction in different pH ranges. Phys. Chem. Chem. Phys. 20 (35), 22890–22901.

Moussout, H., Ahlafi, H., Aazza, M., Bourakhouadar, M., 2016. Kinetics and mechanism of the thermal degradation of biopolymers chitin and chitosan using thermogravimetric analysis. Polym. Degrad. Stab. 130, 1–9.

Nasrollahi, R., Heydari-turkmani, A., Zakavi, S., 2019. Kinetic and mechanistic aspects of solid state, nanostructured porphyrin diacid photosensitizers in photooxidation of sulfides. Cat. Sci. Tech. 9 (5), 1260–1272.

Nichols, E.M., Derrick, J.S., Nistanaki, S.K., Smith, P.T., Chang, C. J., 2018. Positional effects of second-sphere amide pendants on electrochemical CO_2 reduction catalyzed by iron porphyrins. Chem. Sci. 9 (11), 2952–2960.

Panda, N., Sahoo, H., Mohapatra, S., 2011. Decolourization of Methyl Orange using Fenton-like mesoporous Fe_2O_3-SiO_2 composite. J. Hazard. Mat. 185 (1), 359–365.

Parra, S., Nadtotechenko, V., Albers, P., Kiwi, J., 2004. Discoloration of Azo-dyes at biocompatible pH-values through an Fe-histidine complex immobilized on nafion via Fenton-like processes. J. Phys. Chem. B 108 (14), 4439–4448.

Pawar, S.V., Yadav, G.D., 2014. PVA/chitosan-glutaraldehyde cross-linked nitrile hydratase as reusable biocatalyst for conversion of nitriles to amides. J. Mol. Cat. B 101, 115–121.

Quadrado, R.F.N., Fajardo, A.R., 2017. Fast decolorization of azo methyl orange via heterogeneous Fenton and Fenton-like reactions using alginate-Fe^{2+}/Fe^{3+} films as catalysts. Carbohyd. Polym. 177, 443–450.

Rayati, S., Sheybanifard, Z., 2016. Catalytic activity of Mn(III) and Fe (III) porphyrins supported onto multi-walled carbon nanotubes in the green oxidation of organic dyes with hydrogen peroxide: a comparative study. J. Iran. Chem. Soc. 13 (3), 541–546.

Rufus, S.N.A., Philip, D., 2016. Microwave-assisted rapid synthesis of copper nanoparticles with exceptional stability and their multi-faceted applications. J. Mol. Liq. 221, 1008–1021.

Sah, U., Sharma, K., Chaudhri, N., Sankar, M., Gopinath, P., 2018. Antimicrobial photodynamic therapy: Single-walled carbon nanotube (SWCNT)-Porphyrin conjugate for visible light mediated inactivation of Staphylococcus aureus. Colloid Surface B 162, 108–117.

Saltarelli, M., de Faria, E.H., Ciuffi, K.J., Nassar, E.J., Trujillano, R., Rives, V., Vicente, M.A., 2019. Aminoiron(III)-porphyrin-alumina catalyst obtained by non-hydrolytic sol-gel process for heterogeneous oxidation of hydrocarbons. Mol. Cat. 462, 114–125.

Shao, L.J., Hu, B.W., Dong, P.D., Ji, W.X., Qi, C.Z., 2010. Electrospinning Fe(III)porphyrin/TiO_2/poly(styrene) mixture: formation of a novel nanofiber photocatalyst for the photodegradation of methyl orange. J. Porphyrin Phthalocyanine 14 (11), 993–999.

Shi, X.G., Tian, A., You, J.H., Yang, H., Wang, Y.Z., Xue, X.X., 2018. Degradation of organic dyes by a new heterogeneous Fenton reagent-Fe_2GeS_4 nanoparticle. J. Hazard. Mat. 353, 182–189.

Singh, P., Srivastava, V., Quraishi, M.A., 2016. Novel quinoline derivatives as green corrosion inhibitors for mild steel in acidic medium: Electrochemical, SEM, AFM, and XPS studies. Journal of Molecular Liquids 216, 164–173.

Solomon, R.V., Lydia, I.S., Merlin, J.P., Venuvanalingam, P., 2012. Enhanced photocatalytic degradation of azo dyes using nano Fe_3O_4. J. Iran. Chem. Soc. 9 (2), 101–109.

Sonkar, P.K., Prakash, K., Yadav, M., Ganesan, V., Sankar, M., Gupta, R., Yadav, D.K., 2017. Co(II)-porphyrin-decorated carbon nanotubes as catalysts for oxygen reduction reactions: an approach for fuel cell improvement. J. Mater. Chem. A 5 (13), 6263–6276.

Souza, J.F., Costa, G.P., Luque, R., Alves, D., Fajardo, A.R., 2019. Polysaccharide-based superporous hydrogel embedded with copper nanoparticles: a green and versatile catalyst for the synthesis of 1,2,3-triazoles. Cat. Sci. Tech. 9 (1), 136–145.

Synytsya, A., Blafkova, P., Ederova, J., Spevacek, J., Slepicka, P., Kral, V., Volka, K., 2009. pH-Controlled self-assembling of meso-tetrakis(4-sulfonatophenyl)porphyrin-chitosan complexes. Biomacromolecules 10 (5), 1067–1076.

Tagliatesta, P., Crestini, C., Saladino, R., Neri, V., Filippone, P., Fiorucci, C., Attanasi, O.A., 2002. Manganese and iron tetraphenylporphyrin-catalyzed oxidation of a cardanol derivative (hydrogenated tert-butylcardanol). J. Porphyrin Phthalocyanine 6 (1), 12–16.

Thi, D.N., Ngoc, H.P., Manh, H.D., Kim, T.N., 2011. Magnetic Fe_2MO_4 (M:Fe, Mn) activated carbons: Fabrication, characterization and heterogeneous Fenton oxidation of methyl orange. J. Hazard. Mat. 185 (2–3), 653–661.

Ucoski, G.M., Machado, G.S., Silva, G.D., Nunes, F.S., Wypych, F., Nakagaki, S., 2015. Heterogeneous oxidation of the dye Brilliant Green with H_2O_2 catalyzed by supported manganese porphyrins. J. Mol. Cat. A-Chem. 408, 123–131.

Wang, H.F., Zhao, Y.S., Su, Y., Li, T.Y., Yao, M., Qin, C.Y., 2017a. Fenton-like degradation of 2,4-dichlorophenol using calcium peroxide particles: performance and mechanisms. RSC Adv. 7 (8), 4563–4571.

Wang, J.B., Salihi, E.C., Siller, L., 2017b. Green reduction of graphene oxide using alanine. Mat. Sci. Eng. C 72, 1–6.

Wang, L., Jin, P.X., Duan, S.H., Huang, J.W., She, H.D., Wang, Q.Z., An, T.C., 2019. Accelerated Fenton-like kinetics by visible-light-driven catalysis over iron(iii) porphyrin functionalized zirconium MOF: effective promotion on the degradation of organic contaminants. Environ. Sci. Nano 6 (8), 2652–2661.

Wang, R.X., Fan, J.J., Fan, Y.J., Zhong, J.P., Wang, L., Sun, S.G., Shen, X.C., 2014a. Platinum nanoparticles on porphyrin functionalized graphene nanosheets as a superior catalyst for methanol electrooxidation. Nanoscale 6 (24), 14999–15007.

Wang, W., Liu, Y., Li, T.L., Zhou, M.H., 2014b. Heterogeneous Fenton catalytic degradation of phenol based on controlled release of magnetic nanoparticles. Chem. Eng. J. 242, 1–9.

Wei, L.M., Zhang, Y., Chen, S.W., Zhu, L.P., Liu, X.Y., Kong, L.X., Wang, L.J., 2019. Synthesis of nitrogen-doped carbon nanotubes-$FePO_4$ composite from phosphate residue and its application as effective Fenton-like catalyst for dye degradation. J. Environ. Sci. China 76, 188–198.

Xia, Y.J., Wang, G.Q., Guo, L.D., Dai, Q.Z., Ma, X.J., 2020. Electrochemical oxidation of Acid Orange 7 azo dye using a PbO_2 electrode: Parameter optimization, reaction mechanism and toxicity evaluation. Chemosphere 241, 125010.

Yan, Y.Y., Yang, B., Lan, X.Y., Li, X.Y., Xu, F.L., 2019. Cadmium accumulation capacity and resistance strategies of a cadmium-hypertolerant fern - Microsorum fortunei. Sci. Total Environ. 649, 1209–1223.

Yivlialin, R., Bussetti, G., Penconi, M., Bossi, A., Ciccacci, F., Finazzi, M., Duo, L., 2017. Vacuum-deposited porphyrin protective films on graphite: electrochemical atomic force microscopy investigation during anion intercalation. ACS Appl. Mat. Interf. 9 (4), 4100–4105.

Zhang, Y., Zhou, M.H., 2019. A critical review of the application of chelating agents to enable Fenton and 1 Fenton-like reactions at high pH values. J. Hazard. Mat. 362, 436–450.

Zucca, P., Rescigno, A., Pintus, M., Rinaldi, A.C., Sanjust, E., 2012. Degradation of textile dyes using immobilized lignin peroxidase-like metalloporphines under mild experimental conditions. Chem. Central J. 6, 161–168.